SQUID-Detected Liquid State NMR in Microtesla Fields

Andreas H. Trabesinger,[§,†] Robert McDermott,[⊥,‡] SeungKyun Lee,[⊥] Michael Mück,[⊥] John Clarke,[⊥] and Alexander Pines*[,§]

Departments of Chemistry and Physics, University of California, Berkeley, and Materials Sciences Division, Lawrence Berkeley National Laboratory, Berkeley, California 94720

Received: May 1, 2003; In Final Form: November 12, 2003

Nuclear magnetic resonance (NMR) experiments performed in magnetic fields on the order of microtesla yield line widths comparable to the lifetime limit even in grossly inhomogeneous magnets. The potential loss in sensitivity is overcome by combining prepolarization in fields on the order of millitesla and signal detection with a Superconducting Quantum Interference Device (SQUID). The enhanced spectral resolution attainable in microtesla fields enables NMR studies of pure liquids and solutions without the need for strong magnets. We have investigated a variety of heteronuclear systems in both the weak and strong *J*-coupling regimes. Six different nuclear species have been detected with the same experimental apparatus. NMR signals of thermally polarized protons were obtained in fields as low as 554 nT.

Introduction

Throughout the history of nuclear magnetic resonance (NMR) spectroscopy and magnetic resonance imaging (MRI), there has been a drive to higher and higher magnetic field strengths. This drive has been fueled by the need for increased spin polarization, improved detection sensitivity, and broader chemical shift dispersion. Currently the majority of NMR and MRI studies utilize magnetic fields in the range of tesla to tens of tesla.

Nevertheless, since the very early days of NMR, researchers have explored the possibility of performing NMR experiments in much lower magnetic fields, on the order of the Earth's field (∼50 μT). In 1954, the Varian laboratories reported switched fields experiments with detection in the Earth's magnetic field. This initial work encompassed high precision measurements of the strength of the Earth's magnetic field, the simultaneous detection of ^{1}H and ^{19}F signals,[1] as well as relaxation time measurements in low field.[2] These early experiments inspired researchers to study geomagnetism,[3] to perform geophysical investigations of seawater,[4] groundwater,[5] and Antarctic ice,[6] and to evaluate sugar content in plants.[7]

These rather exotic applications involved the investigation of (very) bulky samples that cannot be inserted into a magnet. But in addition they capitalized on instrumental simplicity (compared to high-field setups); it was realized that with relatively inexpensive and easy-to-maintain equipment one can study a variety of NMR phenomena, including *J*-coupling in pure liquids,[8] and relaxation of body fluids.[9] These experiments were considered a useful supplement to high-field NMR, and promised the perspective of making NMR more mobile, taking it out of the traditional laboratory environment.

In the past two decades, low-field MRI applications have attracted particular attention.[10] Apart from the substantial reduction in cost and complexity, advantages here include improved T_1 (longitudinal relaxation time) contrast, as well as the elimination of distortions due to spurious gradients in the case of samples with inhomogeneous magnetic susceptibility.[11]

Despite considerable interest and continued effort, however, low-field NMR remains more of a curiosity than a practical diagnostic tool. The principal obstacle to low-field studies is the inherently low sensitivity. In a conventional pulsed NMR experiment, the static magnetic field serves a dual purpose, as both polarizing field and detection field. This leads to a quadratic dependence of the NMR signal strength on the magnitude B_0 of the static field: for a nuclear moment μ, the thermal magnetization $\mu B_0/k_B T$ scales linearly with the strength of the polarizing field, while the voltage induced in the receiver coil, via Faraday's law, scales with Larmor frequency, and hence with the strength of the detection field. In the majority of previous low-field NMR studies, the low sensitivity often necessitated sample volumes on the order of liters, and thus severely limited the range of possible useful applications. In general, to perform practical NMR experiments in low field it is necessary to address both the problems of low thermal magnetization and the frequency-dependent response of the Faraday detector.

Concepts

In magnetic fields of the order of microtesla, thermal polarizations are extremely small, of the order of 10^{-11}. Nuclear polarizations can be significantly enhanced, however, by prepolarizing the spins in a strong transient field.[12] Prepolarization in a field on the order of millitesla leads to an enhancement of spin magnetization by 3 orders of magnitude. The enhanced magnetization is available in the detection field for a time comparable to T_1. As slight variations in the local polarization over the sample volume have negligible effect on the detected signal, the demands on the homogeneity of the polarization field are insignificant. In comparison with other, nonthermal polarization modalities such as dynamic nuclear polarization (DNP)[13] or optical pumping,[14] thermal prepolarization offers the advantage that *all* NMR-active nuclei are polarized, with Curie's law

* Address correspondence to this author.
§ Department of Chemistry.
⊥ Department of Physics.
† Present address: Physical Chemistry Laboratory, ETH Zurich, Zurich, Switzerland.
‡ Present address: National Institute of Standards and Technology, Boulder, CO 80305.

10.1021/jp035181g CCC: $27.50
Published on Web 01/17/2004

determining the degree of achievable polarization. The time to achieve the final magnetization is dictated by the longitudinal relaxation time T_1.

The consequences of Faraday's law can be circumvented by detection with a Superconducting Quantum Interference Device (SQUID).[15] The dc SQUID consists of a superconducting loop interrupted at two points by Josephson junctions. When appropriately biased with a static current, the voltage across the SQUID oscillates quasisinusoidally as a function of the magnetic flux threading the SQUID loop, with period $\Phi_0 = h/2e$. Thus, the SQUID is a flux-to-voltage transducer. To enhance its sensitivity to magnetic fields, the SQUID is generally operated with a flux transformer, consisting of a pickup coil that is tightly coupled to the sample and an input coil that is tightly coupled to the SQUID loop. In the case of a superconducting flux transformer, which operates on the principle of flux conservation in a closed superconducting loop, the SQUID magnetometer is broadband, and can detect signals at arbitrarily low frequencies without losing sensitivity.

SQUIDs were first used in the 1980s to detect low-field NMR signals (for a review see ref 16). However, the majority of SQUID NMR studies have been performed on samples in the solid state, at liquid helium temperatures. Recently there has been increased interest in extending SQUID NMR techniques to samples in the liquid state, and in particular to systems of biological relevance. Kumar et al.[17] demonstrated NMR spectra from animal tissue measured at room temperature in fields of a few milliteslas. Seton et al.[18] used SQUIDs to image room-temperature samples in a field of 10 mT, and Schlenga et al.[19] used a SQUID magnetometer fabricated from the high transition temperature (T_c) superconductor YBCO to image thermally polarized proton samples at room temperature in a field of 2 mT.

In our experiments we exploit the frequency-independent sensitivity of the SQUID to detect NMR signals in much lower fields, of the order of microtesla. Recently, we demonstrated that NMR detection in microtesla fields—where proton Larmor frequencies are of the order of tens or hundreds of hertz—leads to a reduction in the contribution of inhomogeneous broadening to the point where the line width approaches the lifetime limit even in extremely inhomogeneous fields.[20] The narrowing of the signal band leads to an enhancement of spectral resolution and, in the case of SQUID detection, of the signal-to-noise ratio (SNR).

In this report, we begin with a detailed description of the low-T_c SQUID spectrometer. Further examples are presented which illustrate the various possibilities of obtaining structural information in microtesla fields. Spectra of ^{1}H, ^{2}H, ^{13}C, ^{19}F, ^{31}P, and ^{129}Xe were acquired with the same system. Our initial studies of *J*-coupled systems are extended to heteronuclear systems in the strong coupling regime, demonstrating the potential for applying these techniques to a wide variety of samples. Imaging applications are excluded from the discussion, and will be the subject of a forthcoming paper.

Materials and Methods

Cryogenic Insert. The main design goal for our low-field SQUID NMR spectrometer was to achieve thermal isolation of the room temperature sample from the low-T_c SQUID, which is maintained at liquid helium (LHe) temperature and, at the same time, to obtain a high filling factor. Figure 1 shows our cryogenic insert.

The central compartment of the insert, which is at atmospheric pressure and into which the sample is lowered, has an internal diameter of 22 mm. This compartment is surrounded by a liquid nitrogen (LN_2) jacket with an outer diameter of 100 mm to reduce the heat load of the insert on the LHe bath. In the 80 mm long tail section of the insert, however, the LHe bath is exposed directly to thermal radiation from the inner compartment. The separation of the sample space from the LHe bath in this region is 5 mm. A single, continuous vacuum jacket serves to isolate the central compartment of the insert from the LN_2 jacket (and from the LHe bath in the tail region), and to isolate the LN_2 jacket from the LHe bath; the walls of the vacuum space are silvered, with a slit running the length of the insert.

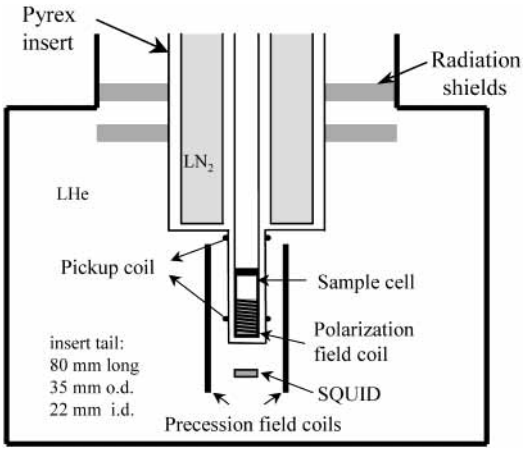

Figure 1. Schematic (not to scale) of the cryogenic insert designed for SQUID-detected liquid-state NMR. For a detailed description see the text.

The upper part of the insert is surrounded by six Styrofoam radiation baffles, which are covered with aluminum foil; these reduce the heat load on the bath due to gaseous convection and direct radiation from the top of the dewar. When the sample is not heated, the system consumes roughly 5 L of LHe per day.

A G-10 fiberglass frame is suspended around the tail section of the insert. This frame supports the SQUID and SQUID pickup circuit, as well as a pair of magnetic field coils, which produce the detection field for NMR experiments.

Detector and Readout. The detector is a low transition temperature dc SQUID operated with an untuned, superconducting input circuit. The pickup coil is configured as a first-order axial gradiometer, with two, two-turn coils wound in the opposite sense and connected in series with the input coil of the SQUID so as to form a superconducting circuit. The pickup loops have a diameter of 38 mm and a baseline of 80 mm, and are wound from 75-μm Nb wire directly on the fiberglass frame. The 11-turn, thin-film Nb input coil is integrated onto the SQUID washer. The SQUID itself is of the Ketchen-Jaycox type,[21] and was fabricated by using an all-liftoff Nb-AlOx-Nb junction technology. The peak-to-peak modulation of the voltage across the SQUID is roughly 40 μV when the device is operated in a well-shielded environment at optimum bias current. The SQUID chip is enclosed in a superconducting lead box. In this way, the SQUID chip and the stray inductance associated with the superconducting contacts in the input circuit are well shielded from external magnetic field fluctuations.

As shown in Figure 2, the SQUID is operated in a flux-locked loop[15] with flux modulation at 2 MHz; the small-signal bandwidth of the loop is about 700 kHz, and the slew rate is greater than 10^6 Φ_0/s at the relevant frequencies. During spin manipulations the feedback loop is disabled by shorting the capacitor across the integrator. The signal from the flux-locked loop passes through a sample-and-hold stage (to remove the

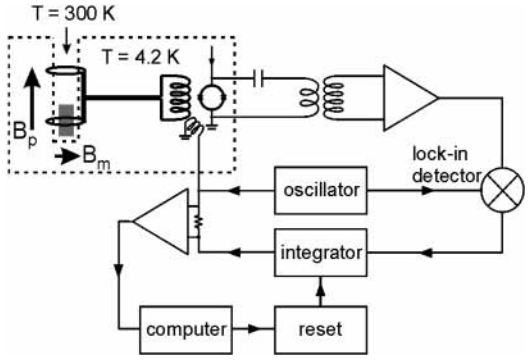

Figure 2. Circuit configuration for detection of low-frequency NMR. The SQUID is operated in a flux-locked loop. The NMR signal is coupled to the SQUID via a superconducting flux transformer configured as an axial gradiometer.

arbitrary offset at the output of the loop) and a set of analogue filters before digitization. Signal averaging is performed in software.

All experiments are performed in a copper mesh Faraday cage to shield the SQUID from radio frequency interference. The belly of the LHe dewar is lined with a superconducting Pb sheet, and the dewar is surrounded by a single-layer mu-metal shield to attenuate the magnetic field of the Earth and external magnetic fluctuations.

Microtesla Field NMR Experiments. To perform the NMR experiments, a Pyrex cell containing the liquid sample is lowered into the tail section of the cryogenic insert; the sample is maintained at a temperature near 300 K with a resistive heater. A polarizing field is applied to the sample by using a single- or double-layer solenoid wound directly on the Pyrex sample cell and oriented along the axis of the SQUID gradiometer. The detection field is provided by a set of coils located in the LHe bath, each consisting of 66 turns of Cu-clad NbTi wire wound on a 90-mm-diameter frame; the separation of the coils is 55 mm.

At the beginning of the pulse sequence, a current of order 1 A is applied to the polarizing coil, generating a field on the order of 1 mT. This polarizing field is maintained for a time that is long compared to the sample T_1 (typically several seconds). At the same time an orthogonally directed field on the order of microtesla is applied via the detection field coils. Nonadiabatic removal of the polarizing field induces precession in the much weaker detection field. Rapid switching of the polarizing field is achieved by closing a field-effect transistor shunt to divert current from the polarizing coil; a reed relay in series with the coil is then opened to prevent coupling of high-frequency interference to the SQUID gradiometer via the polarizing coil. The sudden switching of the polarizing coil induces magnetic transients, apparently due to relaxation of paramagnetic impurities in the Pyrex of the cryogenic insert, which saturate the detector and produce a deadtime on the order of tens of milliseconds. To counteract signal loss due to magnetization dephasing during this time, a spin−echo is employed to refocus the sample magnetization. The echo is formed by reversing the direction of the measurement field, and therefore the sense of precession of the nuclear spins.[20] Field reversal is accomplished simply by energizing a single pole, double throw reed switch that connects the detection coil (and an appropriate series resistor) to either a +12 or −12 V regulated supply.

High-Resolution NMR in Microtesla Fields. In conventional one-dimensional liquid-state NMR, information about the molecules under investigation is obtained primarily from chemical shifts and *J*-couplings.[22] The chemical shift scales with the strength of the externally imposed magnetic field. For ^{1}H, chemical shifts extend to about 10 ppm, while for atoms such as xenon with a large, easily polarized electron cloud, chemical shifts can extend to hundreds or thousands of parts per million. Thus even for a nucleus such as ^{129}Xe with a large chemical shift range, the chemical shifts which occur in microtesla fields ($\sim 10^{-3}$ Hz) are much smaller than the lifetime limited widths of the resonance lines ($\sim$1 Hz); as a result, chemical shift information is lost in such low fields.

By contrast, electron-mediated scalar couplings between nuclei, or *J*-couplings, are field independent. Consequently, *J*-couplings are preserved in microtesla fields, and the strength of the *J*-couplings yields direct information about chemical bonding in a molecule. Due to negligible chemical shifts in microtesla fields the spins of a given nuclear species will always appear equivalent; therefore homonuclear *J*-couplings are not directly observable. In heteronuclear systems, however, the differences between Larmor frequencies in microtesla fields are of the same order of magnitude as the *J*-coupling values. Accordingly, the fine structure of liquid-state spectra in microtesla fields is still resolvable. Typical ranges of heteronuclear *J*-coupling frequencies can be found, for example, in Jardetzky and Roberts.[23]

In general, the character of the *J* spectrum is determined by the relative size of the coupling strength *J* between nuclei and the difference Δ in Larmor frequency of the coupling partners. If the *J*-coupling values are much smaller than the difference in Larmor frequencies (the so-called weak coupling limit), the *J*-coupling Hamiltonian $H_J = 2\pi J\sum\vec{I}\,\vec{S}$ simplifies to $H_J = 2\pi J\sum I_z S_z$ (the sums extend over all spin pairs). The corresponding spectra show the known first-order splittings and their interpretation is straightforward.

The other extreme of strong coupling $J \gg \Delta$ is realized as the strength of the magnetic field is reduced to zero. Whereas the total magnetization of a homonuclear spin system does not evolve under H_J, there is evolution in a heteronuclear system, owing to the different polarizations of unlike spins. Consider for example a *J*-coupled pair of spins $^1/_2$, I and S. The initial density matrix (without constants of motion) in the high-temperature approximation can be written

$$\rho_o = a_I I_x + a_S S_x \tag{1}$$

where $a_x = -(1/Z)\gamma_X B_p/kT$. Here, Z is the partition function of the system, γ_X the magnetogyric ratio of nucleus X, B_p the strength of the polarizing field (assumed to be along the detection direction x), k Boltzmann's constant, and T the absolute temperature. After evolution under H_J for a time t the observable coherences are weighted according to

$$\rho(t) = {}^1/_2[(a_I + a_S) + (a_I - a_S)\cos(2\pi J)]I_x + {}^1/_2[(a_I + a_S) - (a_I - a_S)\cos(2\pi J)]S_x \tag{2}$$

For a homonuclear pair (where $a_I = a_S$), the coefficients of I_x and S_x in (2) are both constant. For a heteronuclear pair, each coefficient oscillates with frequency J, but their sum is again constant. In our experiments, the observable is $(I_x + S_x)$, so that no net oscillation will be seen. However, in the field cycling experiments of Zax et al. the observable was either I_x *or* S_x, and as a result an oscillating signal could be detected.[24] One way to detect a signal in zero field is to break the symmetry with oscillating or static field pulses and acquire the signal point by point. However, this possibility was not explored in this work.

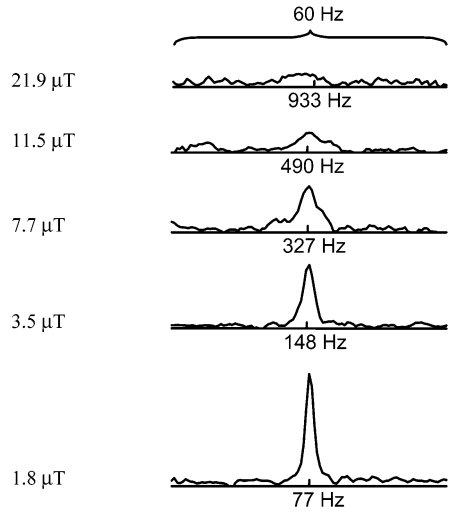

Figure 3. ^{1}H spectra of 5 mL of water (single shot, room temperature). The polarizing field was fixed at ~2 mT, while the measurement field was varied from 21.9 to 1.8 μT. A spectral window of 60 Hz around the proton Larmor frequency is shown at each field strength. All spectra have the same vertical scale. The line narrowing and the accompanying improvement in signal-to-noise ratio are clearly visible.

Finally, if the two interactions enter as equivalent partners, the full Hamiltonian $H = \omega_I I_z + \omega_S S_z + 2\pi J \vec{I}\vec{S}$ (for a spin pair) has to be considered. The terms $2\pi J(I_x S_x + I_y S_y)$ (the so-called flip-flop terms) lead to an oscillatory exchange of magnetization between two coupled spins. The interpretation of the resulting spectra is less intuitive, but can be accomplished by means of analytical or numerical simulations. Some examples are presented later in this paper.

Results

Figure 3 illustrates the effect of line narrowing in low, very inhomogeneous measurement fields.[20] A series of signals was obtained from a 5-mL sample of water. All spectra were acquired without signal averaging in a single shot. The sample was polarized in a field of around 2 mT in all experiments, so that the initial sample magnetization was always the same. The measurement field was varied from 21.9 μT (uppermost trace) to 1.8 μT (lowest trace). Because the detector is untuned, the NMR signal strength—that is, the area under the NMR line—is independent of the strength of the detection field for a fixed sample magnetization. On the other hand, the width of the NMR line is determined by the absolute homogeneity of the detection field, which is enhanced by reduction of the detection field strength. As the detection field strength becomes lower and lower, the NMR lines become narrower and narrower, and the peak height grows. In this way, SQUID detection of the NMR signal in decreasing fields leads to an enhancement of both signal-to-noise ratio (SNR) and spectral resolution. Whereas the signal is not visible in a measurement field of ~20 μT, a clear peak with an SNR of ~10 can be seen upon reducing the measurement field by 1 order of magnitude.

The lowest proton NMR frequency that we measured was 23.6 ± 0.6 Hz, corresponding to a magnetic field of 554 ± 14 nT. Figure 4 displays the spectrum obtained from a 5-mL sample of water after 80 averages. The line width is on the order of 1 Hz, comparable to the natural line width of tap water. The lower limit in field strength is given by the residual background magnetic field due to imperfect screening of the Earth's field by the mu-metal shield surrounding the dewar or to flux trapped in nearby superconducting objects. We measured the component of the residual field along the direction of the measurement field

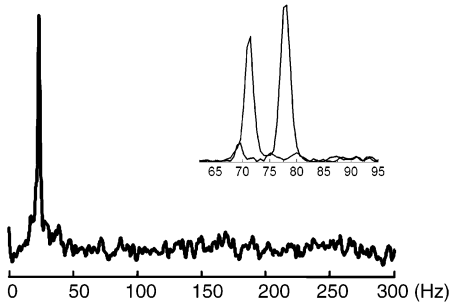

Figure 4. ^{1}H spectrum of 5 mL of water (80 averages, room temperature). The resonance appears at 23.6 ± 0.6 Hz, corresponding to a magnetic field of 554 ± 14 nT. The protons were thermally polarized in a field of ~2 mT. Note that the baseline is flat down to about 1 Hz. The inset shows the two proton spectra obtained with equal and opposite currents in the static field coil that produced fields of ±1.8 μT. The 7-Hz separation of the Larmor frequencies corresponds to a residual field of (7 Hz)/2[42.58 Hz/μT] = 80 nT.

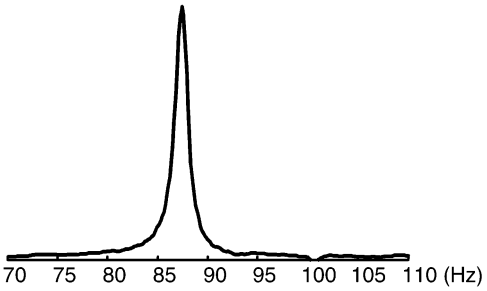

Figure 5. ^{129}Xe spectrum of ~2 mL of hyperpolarized xenon gas at 7.4 μT (1 average, room temperature). An SNR of several hundred and a line width of ~1 Hz are obtained.

by acquiring two proton spectra with opposite currents applied to the measurement field coil as well as by acquiring a series of field reversal spin−echoes with different echo times (only the contribution of the measurement field coils is refocused, but not that of the residual field). Both measurements showed the projection of the residual field onto the direction of the measurement field to be on the order of 100 nT. The residual field seemed to change with each fill of the LHe cryostat, suggesting perhaps different patterns of magnetic flux trapped in the Pb shields.

For the sake of comparison with a nonthermal polarization technique, in Figure 5 we show a spectrum of gaseous xenon, which was hyperpolarized by spin exchange with optically pumped Rb vapor to a polarization of some parts in 1000.[14] The magnetization corresponds roughly to that of liquid water in a field of 1 T. The single shot SNR here was a few hundred; the line width is ~1 Hz.

Earlier,[20] we showed that when phosphoric acid and methanol are esterified the product trimethyl phosphate exhibits a distinct *J*-coupling signature, whereas the reactants do not. The expected first-order spectrum of trimethyl phosphate observed in a field of 6.4 μT consists of a proton line split into a doublet (J^3 = 10.4 ± 0.6 Hz, $J^3/\delta\nu = 0.06$, where $\delta\nu$ is the difference in Larmor frequencies) as shown in Figure 6a. An example of the sensitivity of "pure *J*-spectroscopy" (i.e. without resolved chemical shifts) to molecular structure is given in Figure 6b: Dimethyl methyl phosphonate has a structure very similar to trimethyl phosphate, the only difference being the absence of one oxygen between the phosphorus and one of the three methyl groups (see inset). In the corresponding spectrum, acquired in a field of 3.7 μT, two doublets can be identified, corresponding to the signals arising from the directly bonded methyl group

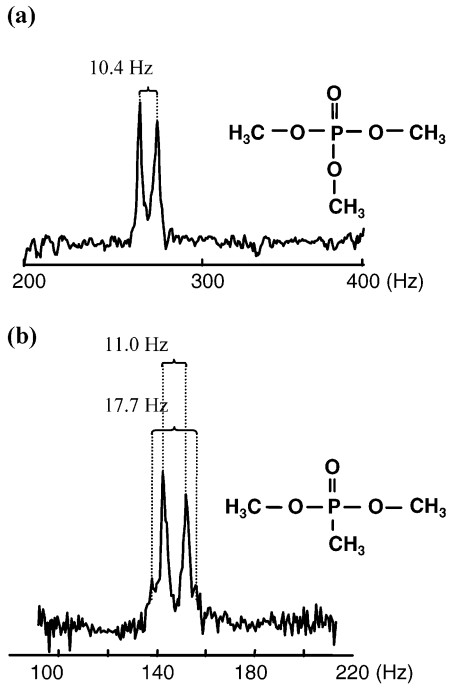

Figure 6. (a) ^{1}H spectrum of 5 mL of trimethyl phosphate at 6.4 μT (735 averages, room temperature, polarizing field ~2 mT). The nine equivalent protons are split into a doublet due to *J*-coupling to the phosphorus nucleus. The coupling constant is 10.4 ± 0.6 Hz. (b) ^{1}H spectrum of 5 mL of dimethyl methyl phosphonate at 3.5 μT (200 averages, room temperature, polarizing field ~2 mT). Two groups of protons are distinguishable: the six equivalent protons with a H−C−O−P coupling are split into a doublet with $J^3 = 11.0 \pm 0.6$ Hz; the three equivalent protons with a H−C−P coupling are split into a doublet with $J^2 = 17.7 \pm 0.6$ Hz. The spectrum still has first-order character. The modulations in the noise at 120 and 180 Hz are due to analogue filters that remove the harmonics of the 60-Hz line signal.

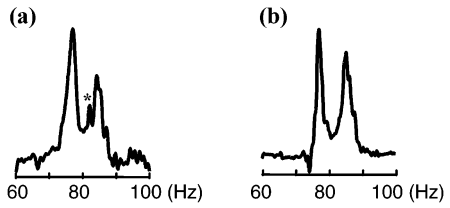

Figure 7. (a) ^{1}H spectrum of 5 mL of dimethyl methyl phosphonate at 1.9 μT (200 averages, room temperature, polarizing field ~2 mT). Strong coupling effects are evident. The peak marked with an asterisk is due to residual water in the sample. (b) Numerical simulation of a ($A_3B + A_6B$) spin system describing dimethyl methyl phosphonate at 1.9 μT ($J^2 = 17.7$ Hz, $J^3 = 11.0$ Hz, $\delta\nu = 48.2$ Hz). The simulated spectrum shows good agreement with the experimental data.

($J^2 = 17.7 \pm 0.6$ Hz) and the two other methyl groups ($J^3 = 11.0 \pm 0.6$ Hz). Although $\delta\nu$ is only a few times larger than *J* ($J^2/\delta\nu = 0.19$; $J^3/\delta\nu = 0.12$), the first-order character of the spectrum is maintained.

However, when the field strength is decreased to 1.9 μT and consequently *J*-coupling becomes stronger relative to the Zeeman interaction ($J^2/\delta\nu = 0.36$, $J^3/\delta\nu = 0.23$), the spectrum of dimethyl methyl phosphonate (Figure 7a) exhibits a more complicated shape. Its interpretation is no longer straightforward; however, the comparison with a numerical simulation (Figure 7b) shows good agreement. The additional peak in the experimental spectrum (marked with an asterisk in Figure 7a) is due to uncoupled spins of residual water in the sample.

When *J*-coupling becomes the dominant term, the spectra again turn out to be relatively simple. An example is depicted

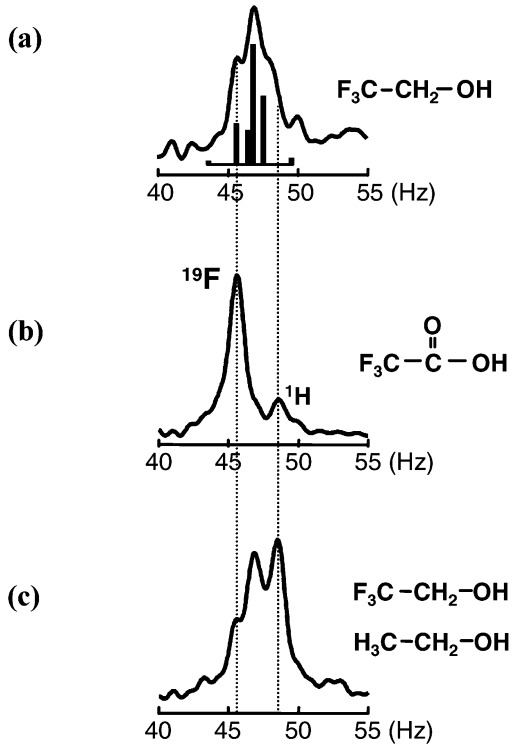

Figure 8. (a) ^{1}H and ^{19}F spectrum of 5 mL of 2,2,2-trifluoroethanol at 1.2 μT (100 averages, room temperature, polarizing field ~2 mT). A second-order spectrum is visible between the frequencies of the uncoupled nuclei (indicated by the dashed lines). The inset shows a stick spectrum of a strongly coupled A_3B_2 spin system in the limit of $J/\delta\nu \rightarrow \infty$. Although $J/\delta\nu$ is only 3.11 in 2,2,2-trifluoroethanol at 1.2 μT, the analytically calculated values show good agreement with the experimental data. (b) ^{1}H and ^{19}F spectrum of 5 mL of 2,2,2-trifluoroacetic acid at 1.2 μT (100 averages, room temperature, polarizing field ~2 mT). The two singlets corresponding to the two isotopes are clearly separated. (c) ^{1}H and ^{19}F spectrum of a 5-mL mixture of 2,2,2-trifluoroethanol and fully protonated ethanol at 1.2 μT (100 averages, room temperature, polarizing field ~2 mT). The additional peak assigned to fully protonated ethanol is clearly distinguishable from the multiplet due to 2,2,2-trifluoroethanol.

in Figure 8a: The spectrum of 2,2,2-trifluoroethanol acquired at 1.1 μT ($J^3 = 8.75$ Hz, $J^3/\delta\nu = 3.11$) extends mainly between the frequencies of the uncoupled fluorines and protons, which are indicated by dashed lines. For comparison we show a spectrum of 2,2,2-trifluoroacetic acid, where the protons and fluorine nuclei show no resolved *J*-coupling (Figure 8b). Figure 8a also shows the stick spectrum expected from analyzing the frequencies contained in the Hamiltonian of a strongly coupled A_3B_2 spin system in the limit of $J/\delta\nu \rightarrow \infty$.[25] In this limit, only 14 out of the total of 34 transitions have nonvanishing intensities and the spectrum consists of six resonance lines. The qualitative agreement with the measured spectrum is good although the approximation $J/\delta\nu \rightarrow \infty$ is rather poor and the intensities of the individual lines are somewhat influenced by the spin−echo. However, in numerical simulations we found that the latter effect is small in the range of echo times we used (on the order of 100 ms). Figure 8c depicts a spectrum of a mixture of 2,2,2-trifluoroethanol and fully protonated ethanol. The good spectral resolution allows for a clear discrimination of the proton singlet of fully protonated ethanol against the multiplet arising from 2,2,2-trifluoroethanol, even though the spectral separation is less than 2 Hz.

Finally we present a first approach to the spectroscopy of solutes. Figure 9 shows the spectrum of an approximately 1 M solution of carbonyl-labeled glycine (see inset) in heavy water,

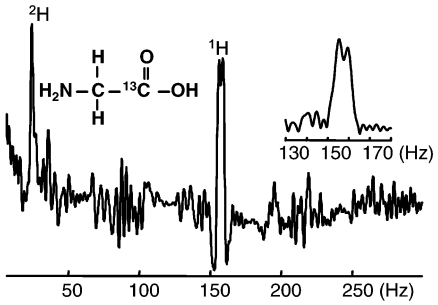

Figure 9. ^{1}H, ^{2}H, and ^{13}C spectrum of 5 mL of a 1 M solution of carbonyl-labeled glycine (see inset) in D_2O at 3.7 μT (5525 averages, room temperature, polarizing field ~2 mT, echo time 167 ms). The two equivalent α-protons are split into a doublet due to *J*-coupling to ^{13}C. The coupling constant is 5 ± 1 Hz as determined by the line shape of the doublet. The second inset displays the proton region of the spectrum in magnitude mode in order to show the doublet structure more clearly. The deuterons of the solvent resonate as a singlet at ~15% of the proton frequency. The ^{13}C triplet that should appear at 40 Hz is below the noise level. The modulations in the noise at integer multiples of 60 Hz are due to analogue filters that remove the harmonics of the 60-Hz line signal.

acquired in a field of 3.7 μT with an echo time of 167 ms. A *J*-modulated doublet centered at 158 Hz is discernible, with a line shape consistent with a coupling strength $J^2 = 5 \pm 1$ Hz. In addition, a singlet due to deuterium is evident at 24 Hz. The relative intensity of the lines from the two hydrogen isotopes is determined only by their respective spin densities and differences in thermal equilibrium magnetization (proportional to $\gamma^2 I(I + 1)$, where γ is the magnetogyric ratio and I the spin quantum number). The detection sensitivity is the same for the two isotopes.

Discussion

Following the demonstration of high-resolution spectra in microtesla fields,[20] this article is intended to show the versatility of "pure *J*-spectroscopy", i.e., spectroscopy in a regime where chemical shifts are not resolved. Using various examples, we have shown that *J*-coupling alone creates spectral signatures that allow one to identify molecules in microtesla fields. Thus, the method described is potentially useful as a "bond detector" that could be applied to the study of analytes, chemical reactions, and molecular conformations. The high spectral resolution provides the means to acquire accurate information about scalar couplings. This information allows one to discriminate different molecular groups, as shown for dimethyl methyl phosphonate (Figure 6). The experiment with amino acid glycine in aqueous solution (Figure 9) suggests the possibility of performing NMR without a high-field magnet in biological research. In view of the highly developed techniques for isotopic labeling in biomolecular and biomedical NMR, the use of such a method for following a "spy nucleus" through bond formation is an appealing prospect.

Compared to the pioneering experiments,[1,8,9] our samples are 2 to 3 orders of magnitude smaller and can be kept at temperatures ranging from close to 4.2 K to above room temperature. These two advantages seem essential for practical applications. Whereas traditionally low-field NMR is practiced in situations where it is impractical or impossible to place the sample in a high-field magnet, the results presented here indicate that spectroscopic investigation of a few grams of substance is possible in microtesla fields. This will be of interest in situations where the sensitivity and detailed information obtained in well-shimmed high-field magnets is not necessarily needed.

Since our SQUID magnetometer is operated with an untuned input circuit, detection is broadband. Moreover, the pulse sequence employed in our experiments involves switched static fields rather than resonant spin manipulation; thus excitation also occurs over a broad band. Our experimental technique is therefore ideally suited to studies of systems containing nuclei with different magnetogyric ratios. A spectrum containing phosphorus and proton resonances was shown previously.[20] In the current article, we show the simultaneous detection of protons and deuterons (Figure 9) as well as a spectrum featuring protons and fluorine nuclei (Figure 8). The ability to perform multinuclear studies without changing the measurement system is an important feature of our instrumentation.

The data presented here are an expansion of former results showing resolved *J*-coupling in the weak coupling regime. They demonstrate how the concept of "pure *J*-spectroscopy" can be expanded to a broader class of samples. It is a well-known fact in NMR that spectra become considerably simpler if one enters the weak coupling regime. This factor is one of the reasons why recent decades saw the development of ever stronger magnets for NMR. The examples shown here (Figure 8) demonstrate that in the "very strong coupling regime" the spectra once again become more readable, although their interpretation is still not as straightforward as for first-order spectra. However, analytical and numerical simulations proved to be very useful (Figures 7 and 8), and at least may allow one to narrow the range of possible conformations if the structure is not known. In addition, Figures 6b and 7a give examples in which varying the field strength and hence the ratio $J/\delta\nu$ allows the experimenter to tune to a favorable ratio $J/\delta\nu$. Such tuning is easily achieved given the small magnetic fields involved.

Acknowledgment. We are grateful to Herbert Zimmermann for discussions and providing labeled samples, to Tom Lawhead for expert glassblowing and advice, and to Megan M. Spence and Adam J. Moulé for advice and assistance with the xenon experiments. This work was supported by the Director, Office of Science, Office of Basic Energy Sciences, Materials Science and Engineering Division, U.S. Department of Energy under Contract No. DE-AC03-76SF00098.

References and Notes

(1) Packard, M.; Varian, R. *Phys. Rev.* **1954**, *93*, 941.
(2) Bloom, A.; Mansir, D. *Phys. Rev.* **1954**, *93*, 941.
(3) Waters, G. S. *Nature* **1955**, *176*, 691.
(4) Hahn, E. L. *J. Geophys. Res.* **1960**, *65*, 776.
(5) Shushakov, O. A. *Magn. Reson. Imaging* **1996**, *14*, 959.
(6) Callaghan, P. T.; Eccles, C. D.; Haskell, T. G.; Langhorne, P. J.; Seymour, J. D. *J. Magn. Reson.* **1998**, *133*, 148.
(7) Eustace, C. A.; Jordan, R. B. *Trans. ASAE* **1995**, *38*, 1563.
(8) Elliott, D. F.; Schumacher, R. T. *J. Chem. Phys.* **1957**, *26*, 1350. Thompson, D. D.; Brown, R. J. S. *J. Chem. Phys.* **1961**, *35*, 1894. Thompson, D. D.; Brown, R. J. S. *J. Chem. Phys.* **1962**, *36*, 2812. Thompson, D. D.; Bloom, M.; Brown, R. J. S. *J. Chem. Phys.* **1964**, *40*, 3076.
(9) Bene, G. J. *Phys. Rep.-Rev. Sect. Phys. Lett.* **1980**, *58*, 213.
(10) Mehier, H.; Maurice, M.; Bonche, J. P.; Jacquemod, G.; Desuzinges, C.; Favre, B.; Peyrin, J. O. *J. Biophys. Biomec.* **1985**, *9*, 198. Favre, B.; Bonche, J. P.; Mehier, H.; Peyrin, J. O. *Magn. Reson. Med.* **1990**, *13*, 299. Stepisnik, J.; Erzen, V.; Kos, M. *Magn. Reson. Med.* **1990**, *15*, 386. Stepisnik, J.; Kos, M.; Planinsic, G.; Erzen, V. *J. Magn. Reson. Ser. A* **1994**, *107*, 167. Planinsic, G.; Stepisink, J.; Kos, M. *J. Magn. Reson. Ser. A* **1994**, *110*, 170. Mohoric, A.; Stepisnik, J.; Kos, M.; Planinsic, G. *J. Magn. Reson.* **1999**, *136*, 22.
(11) Tseng, C. H.; Wong, G. P.; Pomeroy, V. R.; Mair, R. W.; Hinton, D. P.; Hoffmann, D.; Stoner, R. E.; Hersman, F. W.; Cory, D. G.; Walsworth, R. L. *Phys. Rev. Lett.* **1998**, *81*, 3785. Wong-Foy, A.; Saxena, S.; Moule, A. J.; Bitter, H. M. L.; Seeley, J. A.; McDermott, R.; Clarke, J.; Pines, A. *J. Magn. Reson.* **2002**, *157*, 235.

(12) Macovski, A.; Connolly, S. *Magn. Reson. Med.* **1993**, *30*, 221. Shao, W.; Wang, G.; Fuzesy, R.; Hughes, E. W.; Chronik, B. A.; Scott, G. C.; Connolly, S. M.; Macovski, A. *Appl. Phys. Lett.* **2002**, *80*, 2032.

(13) Abragam, A.; Goldman, M. *Nuclear Magnetism*: *Order and Disorder*; Clarendon: Oxford, UK, 1982. Slichter, C. P. *Principles of Nuclear Magnetic Resonance*, 3rd ed.; Springer-Verlag: New York, 1990.

(14) Goodson, B. M. *J. Magn. Reson.* **2002**, *155*, 157.

(15) Clarke, J. In *SQUID Sensors*: *Fundamentals, Fabrication and Applications*; Weinstock, H., Ed.; Kluwer Academic: Dordrecht, The Netherlands, 1996; p 1.

(16) Greenberg, Y. S. *Rev. Mod. Phys.* **1998**, *70*, 175.

(17) Kumar, S.; Thorson, B. D.; Avrin, W. F. *J. Magn. Reson. Ser. B* **1995**, *107*, 252.

(18) Seton, H. C.; Hutchison, J. M. S.; Bussell, D. M. *Meas. Sci. Technol.* **1997**, *8*, 198.

(19) Schlenga, K.; McDermott, R.; Clarke, J.; de Souza, R. E.; Wong-Foy, A.; Pines, A. *Appl. Phys. Lett.* **1999**, *75*, 3695.

(20) McDermott, R.; Trabesinger, A. H.; Muck, M.; Hahn, E. L.; Pines, A.; Clarke, J. *Science* **2002**, *295*, 2247.

(21) Jaycox, J. M.; Ketchen, M. B. *IEEE Trans. Magn.* **1981**, *17*, 400.

(22) Ernst, R. R.; Bodenhausen, G.; Wokaun, A. *Principles of Nuclear Magnetic Resonance in One and Two Dimensions*; Oxford University Press: Oxford, UK, 1987.

(23) Jardetzky, O.; Roberts, G. C. K. NMR In *Molecular Biology*; Academic: New York, 1981.

(24) Zax, D. B.; Bielecki, A.; Zilm, K. W.; Pines, A. *Chem. Phys. Lett.* **1984**, *106*, 550.

(25) Corio, P. L. *Structure of High-Resolution NMR Spectra*; Academic Press: New York, 1966.